The role of electron-driven microinstabilities in particle transport during electron Internal Transport Barriers

E. Fable[1], C. Angioni[2], A. Bottino[2], S. Brunner[1], T. Dannert[2], F. Jenko[2], O. Sauter[1]

[1]*Ecole Polytechnique Fédérale de Lausanne (EPFL)*
Centre de Recherches en Physique des Plasmas (CRPP)
Association EURATOM - Confédération Suisse CH - 1015 Lausanne, Switzerland
[2]*Max-Planck-Institut für Plasmaphysik, EURATOM Association, 85748 Garching, Germany*

Abstract

Experimental results obtained in TCV electron Internal Transport Barriers (eITBs) show a strong coupling between the plasma density and the electron temperature logarithmic gradients [1]. The plasma density is sustained by an inward thermodiffusive pinch whose theoretical understanding has not been achieved yet. The level of particle diffusivity, as estimated in transient transport experiments, indicates anomalous transport as the main mechanism to create this pinch. On the other hand, a clear improved heat and particle transport confinement is observed. Gyrokinetic calculations of the pinch coefficients are performed in the framework of quasi-linear theory neglecting core particle sources and impurities. The role of non-adiabatic passing electrons is taken into account and shown to be negligible, as well as the so called turbulent equipartition pinch. The coupling between density and temperature is provided via trapped electrons driven thermodiffusion which is maximized near the transition between ITG-dominated to TEM-dominated turbulence. This regime is obtained in a plasma characterized by large temperature and density logarithmic gradients through different stabilizing mechanisms discussed here.

Introduction

Peaked density profiles are usually observed during the steady-state operation of eITBs in TCV [1]. The density logarithmic gradient is found to be correlated with the electron temperature logarithmic gradient with a robust, in the sense of experimental reproduction, ratio of about 0.4-0.5 , i.e. $R/L_{\mathrm{n}} \sim 0.45R/L_{\mathrm{Te}}$. Neoclassical transport is still negligible in these eITB scenarios [2] and thus we will resort to turbulence codes to elucidate the background physics. The gyrokinetic code GS2 [3] is employed to understand how steady-state density profiles are sustained by the anomalous pinch for typical eITB parameters. The eITB scenario discussed here involves the reversal of the magnetic shear and very strong electron heating, assessing the role of the Trapped Electron Mode (TEM) that is usually associated with flattened density profiles [4].

Theoretical background

The steady-state density profile, in the framework of quasi-linear turbulence theory, is given by the general formula:

$$\frac{R}{L_{\mathrm{n}}} = -R\frac{V}{D} = -C_{\mathrm{T}}\frac{R}{L_{\mathrm{Te}}} - C_{\mathrm{P}} \Rightarrow \sigma_{\mathrm{e}} = \frac{1}{\eta_{\mathrm{e}}} = \frac{L_{\mathrm{Te}}}{L_{\mathrm{n}}} = -C_{\mathrm{T}} - C_{\mathrm{P}}\frac{L_{\mathrm{Te}}}{R} \tag{1}$$

where V and D are the pinch velocity and diffusion coefficient respectively. The term $-C_{\mathrm{T}}\frac{R}{L_{\mathrm{Te}}}$ is called turbulent thermodiffusion (THD), while the other off-diagonal term has been historically called 'turbulent equipartition' (TEP) [5]; in this context the latter contains all the off-diagonal contributions to particle transport which are not linearly proportional to R/L_{Te}. The two coefficients are evaluated with GS2 via a trace-particle method solving a linear system to find C_{T} and

C_P. Note that for a single ballooning mode (identified by the value of the poloidal wavenumber $k_y\rho_\mathrm{i}$) the two coefficients are *independent* of the mixing length rule for $|\Phi|^2$ (i.e. the turbulence level determines fluxes but not source-less steady-state profiles), allowing a more stringent comparison with the experiment without assumptions on non-linear saturation phenomena. The sign convention, as seen from Eq.(1), is such that negative values of the coefficients give inward pinch contribution, while positive values contribute outward. Without trapping it is possible to evaluate analytically the thermodiffusion coefficient for electrons to be $-C_\mathrm{T} \approx 0.5$, in agreement with the experimental observations. However, the trapped fraction is $f_\mathrm{t} \sim 0.4$ at mid-radius where the maxima of the logarithmic gradients are usually located. Trapped electrons contribute with a strong outward pinch for a mode rotating in the electronic direction, almost reversing the sign of C_T for a strong TEM. We therefore expect the TEM to be marginally stable for the particle barrier to exist. As will be shown later: $C_\mathrm{P} \ll C_\mathrm{T}\frac{R}{L_\mathrm{Te}}$, allowing us to concentrate on the behavior of C_T only.

Understanding the density barrier

The GS2 simulations are done with input parameters from #29859, a typical eITB obtained in TCV: $R/L_\mathrm{Te} = 16$, $T_\mathrm{e}/T_\mathrm{i} = 2.5$, $\hat{s} = -0.7$, $q = 2.7$, $\varepsilon = 0.11$, $\alpha_\mathrm{MHD} \approx 1.5$. R/L_n is scanned to find the self-consistent steady-state point of zero particle flux. R/L_Ti and α_MHD are varied to

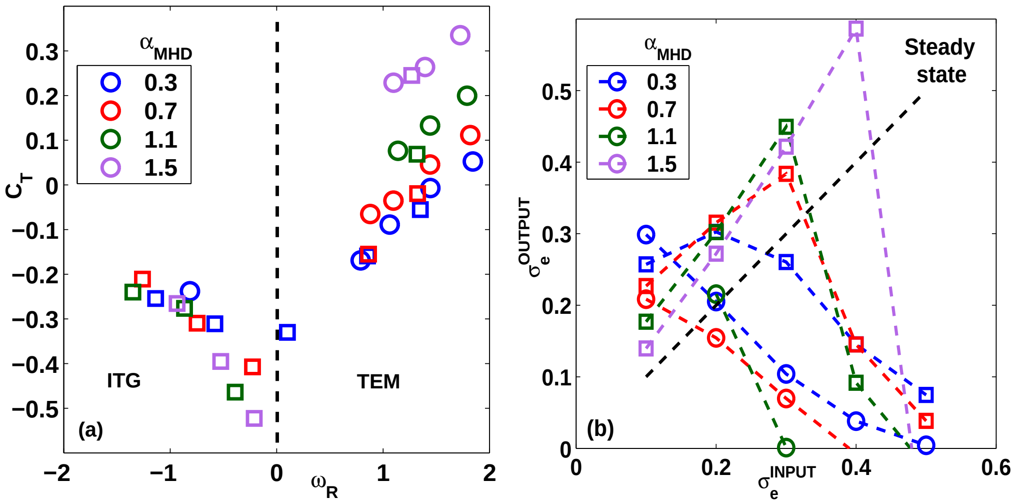

Figure 1: **a**) Thermodiffusion coefficient C_T versus the mode frequency ω_R for different values of α_MHD obtained with GS2, circles represent $L_\mathrm{Te}/L_\mathrm{Ti} = 0.5$ and squares $L_\mathrm{Te}/L_\mathrm{Ti} = 0.8$; **b**) Steady-state diagram for $\sigma_\mathrm{e} = L_\mathrm{Te}/L_\mathrm{n}$: $\sigma_\mathrm{e}^{\mathrm{OUTPUT}_\mathrm{GS2}} > \sigma_\mathrm{e}^{\mathrm{INPUT}_\mathrm{GS2}}$ implies an inward flux and subsequent increase of σ_e, $\sigma_\mathrm{e}^{\mathrm{OUTPUT}} < \sigma_\mathrm{e}^{\mathrm{INPUT}}$ implies an outward flux, $\sigma_\mathrm{e}^{\mathrm{OUTPUT}} = \sigma_\mathrm{e}^{\mathrm{INPUT}}$ (black dashed) provides the steady-state value when intersecting the different curves (the intersections are *stable* steady-state points)

test the response of TEMs and their stabilization. The normalized poloidal wavenumber is fixed at $k_y\rho_\mathrm{i} = 0.3$ where the spectrum of $\gamma/ < k_\perp^2 >$ peaks for these parameters (quasi-linear rule, see [6]). We neglect impurity physics assuming $Z_\mathrm{eff} = 1$, reminding that in the experimental discharges analyzed we observe a global $Z_\mathrm{eff} \sim 3$. The calculations are made in the electrostatic ($\beta_\mathrm{T} \sim 10^{-3}$) and collisionless limit, without core particle sources. The simulations indicate that C_T is maximized, in the inward direction, around the ITG-TEM transition, i.e. when $\omega_\mathrm{R} \lesssim 0$, figure 1(a). The maximum value of $-C_\mathrm{T}$ increases with α_MHD, which is thus a favorable parameter. We note also that a higher α_MHD gives a sharper transition in the behavior of C_T. Figure 1(b) shows how to identify the self-consistent steady-state point: $\sigma_\mathrm{e}^{\mathrm{INPUT}}$ represents the value of R/L_n (R/L_Te is fixed) given as input to the code. $\sigma_\mathrm{e}^{\mathrm{OUTPUT}}$ is calculated from Eq.(1)

using C_T and C_P as obtained by the code. If $\sigma_e^{OUTPUT} \neq \sigma_e^{INPUT}$ it means that the particle flux is different from zero and it is directed inward if $\sigma_e^{OUTPUT} > \sigma_e^{INPUT}$ and outward if $\sigma_e^{OUTPUT} < \sigma_e^{INPUT}$. The steady-state points, stables if $\left[d\sigma_e^{OUTPUT}/d\sigma_e^{INPUT} < 1\right]_{\sigma_e=\sigma_e^{Steady-state}}$, are located at the intersection of the calculated curves and the $\sigma_e^{OUTPUT} = \sigma_e^{INPUT}$ line. At high values of α_{MHD} the steady-state point moves towards higher values of σ_e, but it appears as a 'threshold' phenomena rather than a continuous process. R/L_{Ti} seems to be fundamental in providing a more efficient effect of α. Figure 2(a) shows the real frequency ω_R for the most unstable mode

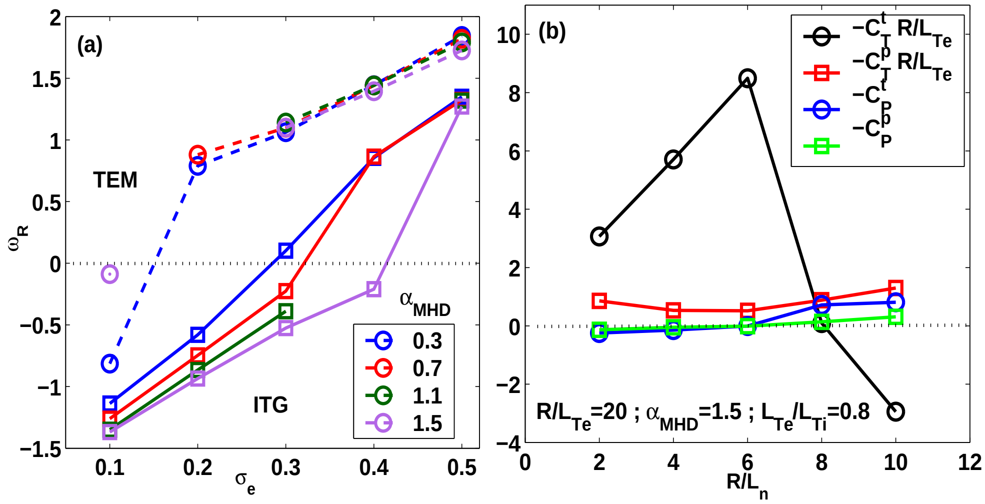

Figure 2: **a**) Most unstable mode ω_R versus σ_e. Solid-squares for $L_{Te}/L_{Ti} = 0.5$ and dashed-circles for $L_{Te}/L_{Ti} = 0.8$; **b**) Pinch coefficients C_T and C_P divided into trapped (C_T^t and C_P^t) and passing (C_T^p and C_P^p) electrons contributions versus R/L_n for one specific case.

versus σ_e. The transition from ITG to TEM occurs near $\omega_R = 0$. This point shifts towards higher σ_e with an increase of the value of α_{MHD} and L_{Te}/L_{Ti} (squares vs circles). Figure 2(b) shows the two pinch terms $-C_T \frac{R}{L_{Te}}$ and C_P divided into trapped and passing particles contribution. The TEP coefficient C_P is found to be negligible, as well as the contribution of passing electrons. The dominant part of the pinch comes from trapped particles driven thermodiffusion.

Combined s-α_{MHD} effect

The barrier existence is provided by the stabilizing effect of both reversal of magnetic shear s and increased plasma pressure via the α_{MHD} parameter [7]. The magnetic curvature drift in the ballooning formalism is expressed as: $\omega_D \approx \cos\theta + (s\theta - \alpha\sin\theta)\sin\theta$, which for $\theta \sim 0$ becomes $\omega_D \approx 1 + (s - \alpha - 1/2)\theta^2$. Stabilization becomes stronger as the parabola becomes more 'peaked', i.e. as $|s - \alpha - 1/2| \Rightarrow \infty$. However, the efficiency of $s - \alpha$ in changing the mode real frequency ω_R depends on the value of L_{Te}/L_{Ti}, while the growth rate seems to decrease similarly in the two cases. In figure 3 we see that, at fixed gradients, the mode is more and more stable combining magnetic shear reversal and increasing Shafranov shift. The mode being a TEM at small absolute values of $s - \alpha_{MHD}$, it switches to ITG when $s - \alpha_{MHD}$ stabilization is sufficiently strong. It requires either a large negative shear or a large Shafranov shift. The transition from ITG-dominated to TEM-dominated turbulence is provided by $s - \alpha_{MHD}$ stabilization of TEM and a value of $L_{Te}/L_{Ti} \lesssim 1$. It is interesting to note that, contrary to the temperature barrier which is due to a decrease in the heat flux at constant input power, linked to the decrease of the mode growth rate γ, the density barrier sustainment is strongly related to the behavior of the mode frequency ω_R and much less on the value of γ.

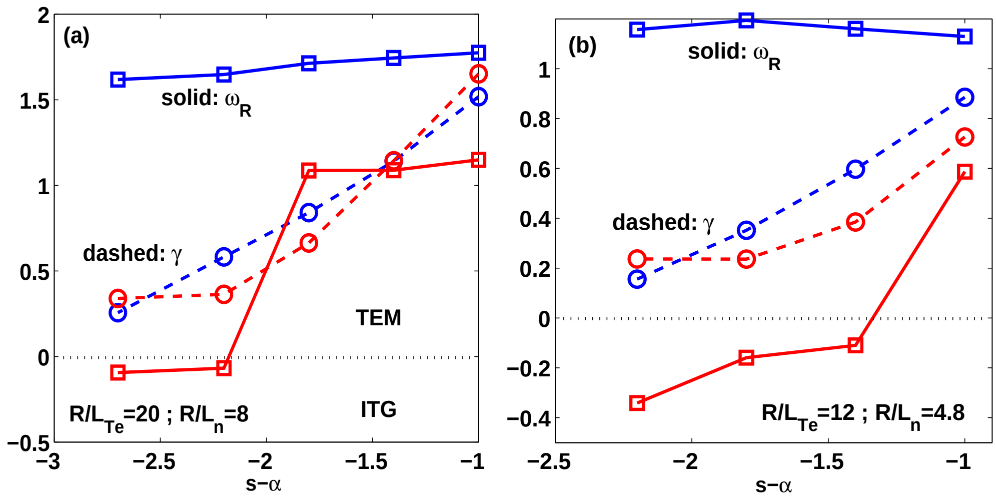

Figure 3: Growth rate γ (dashed) and frequency ω_R (solid) versus $(s - \alpha_{\mathrm{MHD}})$ for two cases: $L_{\mathrm{Te}}/L_{\mathrm{Ti}} = 0.5$ (blue) and $L_{\mathrm{Te}}/L_{\mathrm{Ti}} = 0.8$ (red). Shear is fixed at $s = -0.7$.

The role of impurities, collisionality and ions

Preliminary results show that TEMs are more unstable due to the impurity driver for values of $Z_{\mathrm{eff}} > 2$, and thus the density logarithmic gradient is diminished. Collisionality seems to play a similar role in decreasing the efficiency of trapped particles in carrying the thermodiffusive inward pinch. Ions experimental parameters are presently unknown; to make a quantitative comparison with theory, a future experimental TCV campaign will be devoted to this issue.

Discussion of the results

The gyrokinetic simulations of particle transport in this eITB scenario are consistent with the observed density if conditions are met such that turbulence is near the ITG-TEM transition. The experimental results show that R/L_n is sustained by a dominant anomalous thermodiffusive inward pinch [1]. This inward pinch is maximized at the ITG-TEM transition, i.e. when the mode real frequency ω_R approaches zero, and the pinch coefficient C_T is found to be consistent with the experimental values. We have shown that C_T is only due to trapped particles. The TEP and the passing particles contributions are negligible. The combination of negative magnetic shear and high values of α_{MHD} stabilize the TEM and can shift the ITG-TEM transition point to higher values of R/L_n near the experimental values. The ion to electron temperature logarithmic gradients ratio is also important since it affects directly the ITG contribution. Values of order $L_{\mathrm{Te}}/L_{\mathrm{Ti}} \lesssim 1$ are required.

Acknowledgements

This work was supported in part by the Swiss National Science Foundation.

References

[1] E. Fable *et al.*, *Plasma Phys. Contr. Fus.* **48**, 1-13 (2006)
[2] E. Fable *et al.*, *Theory of Fusion Plasmas*, AIP Conference Proceedings **871**, 318-323 (2006)
[3] M. Kotschenreuther *et al.*, *Comput. Phys. Commun.* **88**, 128 (1995)
[4] C. Angioni *et al.*, *Nucl. Fusion* **44**, 827 (2004)
[5] D. R. Baker and M. N. Rosenbluth, *Phys. Plasmas* **5**, 2936 (1998)
[6] F. Jenko *et al.*, *Plasma Phys. Contr. Fus.* **47**, B195 (2005)
[7] A. Bottino *et al.*, *Plasma Phys. Contr. Fus.* **48**(2), 215 (2006)